Imaging Coronary Artery Microstructure Using Second-Harmonic and Two-Photon Fluorescence Microscopy

Aikaterini Zoumi,* Xiao Lu,† Ghassan S. Kassab,† and Bruce J. Tromberg*†
*Laser Microbeam and Medical Program, Beckman Laser Institute, and †Center for Biomedical Engineering, University of California, Irvine, California

ABSTRACT The microstructural basis for the mechanical properties of blood vessels has not been directly determined because of the lack of a nondestructive method that yields a three-dimensional view of these vascular wall constituents. Here, we demonstrate that multiphoton microscopy can be used to visualize the microstructural basis of blood vessel mechanical properties, by combining mechanical testing (distension) of excised porcine coronary arteries with simultaneous two-photon excited fluorescence and second-harmonic generation microscopy. Our results show that second-harmonic generation signals derived from collagen can be spectrally isolated from elastin and smooth muscle cell two-photon fluorescence. Two-photon fluorescence signals can be further characterized by emission maxima at 495 nm and 520 nm, corresponding to elastin and cellular contributions, respectively. Two-dimensional reconstructions of spectrally fused images permit high-resolution visualization of collagen and elastin fibrils and smooth muscle cells from intima to adventitia. These structural features are confirmed by coregistration of multiphoton microscopy images with conventional histology. Significant changes in mean fibril thickness and overall wall dimension were observed when comparing no load (zero transmural pressure) and zero-stress conditions to 30 and 180 mmHg distension pressures. Overall, these data suggest that multiphoton microscopy is a highly sensitive and promising technique for studying the morphometric properties of the microstructure of the blood vessel wall.

INTRODUCTION

The mechanical properties of blood vessels modulate a broad variety of phenomena, including pressure, flow, stress, and mass transport that, in turn, have a critical impact on cardiovascular function in health and disease (Mulvany, 1984). Vessel mechanical properties stem from microstructural wall components, such as collagen and elastin fibers, and smooth muscle cells (Roach and Burton, 1957; Oka, 1968, 1972, 1981; Oka and Azuma, 1970; Azuma and Hasegawa, 1971; Azuma and Oka, 1971). These microstructural components have different mechanical properties and take up loads at different stress levels. Consequently, blood vessels are known to exhibit complex and difficult to predict mechanical behavior (Fung, 1990).

Previous attempts to determine morphometric features, such as diameter, length, number density, orientation, and curvature of collagen and elastin fibers, have generally employed destructive differential digestion techniques. These approaches have failed to provide useful data because the fibers are so dense that it is difficult to make measurements. The major reason for the lack of progress in this area is the lack of a technique that yields a three-dimensional rendering of the structure of collagen, elastin, and smooth muscle cells.

Multiphoton microscopy (MPM) is a biological imaging technique that relies on nonlinear light-matter interactions to provide high contrast and optical sectioning capabilities. The nonlinear signals responsible for forming images in multiphoton microscopy are of two primary types (Zoumi et al., 2002): second-harmonic generation (SHG) and two-photon excited fluorescence (TPF). Both types of nonlinear interactions occur in biological tissues without the addition of exogenous contrast agents. Two-photon excited fluorescence has been widely used for imaging cells and tissues (Denk et al., 1990; Masters et al., 1997, 1998; So et al., 1998; Squirrell et al., 1999; Diaspro and Robello, 2000; Agarwal et al., 2001; Masters and So, 2001). Second harmonic generation has recently been employed for biological imaging applications (Guo et al., 1997; Gauderon et al., 1998; Campagnola et al., 1999; Georgiou et al., 2000; Moreaux et al., 2000b). The combination of TPF and SHG has been implemented for the study of cells (Campagnola et al., 1999, 2001; Moreaux et al., 2000a, 2001; Gauderon et al., 2001), thin tissue sections (Campagnola et al., 2002), and for the more practical case of thick, unstained living specimens (Guo et al., 1999; Zoumi et al., 2002).

Collagen is a well-documented source of tissue SHG (Roth and Freund, 1981; Georgiou et al., 2000; Campagnola et al., 2001), and autofluorescence (Richards-Kortum and Sevick-Muraca, 1996; Masters and So, 1999; Agarwal et al., 2001). Elastin is also a significant source of extracellular matrix autofluorescence (Richards-Kortum and Sevick-Muraca, 1996). Collagen and elastin are important determinants of the mechanical properties of blood vessels. Their selective visualization is of fundamental interest for the determination of the microstructural origins of mechanical properties. Fluorescence emission can provide a possible method to separate tissue constituents based on differential spectral features. In the case of collagen and elastin, however,

Submitted March 18, 2004, and accepted for publication July 1, 2004.
Address reprint requests to B. J. Tromberg, E-mail: tromberg@bli.uci.edu.

0006-3495/04/10/2778/09 $2.00
doi: 10.1529/biophysj.104.042887

the emission spectra overlap significantly (Richards-Kortum and Sevick-Muraca, 1996), thus rendering their characterization a difficult task.

Here, we use TPF and SHG in tandem to accomplish the selective visualization of the structural components of elastic and muscular arteries. We also combine distension of coronary arteries with the simultaneous determination of collagen, smooth muscle cell, and elastin structure. Specifically, we use combined TPF and SHG microscopy to selectively monitor the structural changes of collagen, elastin, and smooth muscle cells in response to different loading conditions. This approach will establish a microstructural foundation for the observed mechanical properties of blood vessels and shows the potential of MPM as a noninvasive technique for the characterization of vascular physiology and pathology.

MATERIALS AND METHODS

Blood vessel preparation

Rabbit aortas and pig coronary arteries were used in this study. Rabbit aortic specimens were excised and fixed in formaline. Five hearts of Danish Landrace-Yorkshire pigs with body weight in the range of 90–95 Kg were obtained at a local slaughterhouse. The hearts were transported to the laboratory in 4°C Krebs solution within 15 min after the animal was sacrificed. The left anterior descending (LAD) artery and right coronary artery (RCA) were dissected carefully from their emergence at aortic ostia. The adjacent tissue around the segments was dissected carefully in cool Krebs solution.

Distension protocol

For each coronary artery sample a segment of ~1 cm in length was used for distension. A custom-made balloon tip catheter was inserted into the lumen of the coronary artery and distended to the desired pressure. The balloon has excess surface area such that the entire pressure load is transmitted to the vessel wall, i.e., no tension is taken up by the balloon itself. For each of the two coronary arteries, LAD and RCA, coronary segments were prepared under four different stress and strain conditions: 1), zero-stress state; 2), no-load (zero-transmural pressure) state; 3), 30-mmHg distension; and 4), 180-mmHg distension. The zero-stress state was obtained by cutting the no-load state radially, which caused it to spring open releasing all residual stresses and strains (Fung, 1984; Lu et al., 2001). Immediately after distension and before releasing the vessel from the balloon, the vessel was immersion-fixed in 6.25% Glutaraldehyde to preserve the mechanical state.

Combined SHG/TPF imaging of vessels

Immediately after excision of the rabbit aorta 2 mm-thick cross-section rings were sectioned from the vessel. Some of the rings were imaged fresh and some were fixed in 4% formaline to be imaged later. Immediately after imposing distension and fixing the coronary arteries to preserve their loading state, ~2 mm-thick cross-section rings were sectioned from the vessel segments using a tissue chopper. MPM images and spectra from the cross-section rings were obtained using a combined SHG/TPF setup that has been previously described (Zoumi et al., 2002). All images and spectra shown were obtained for an excitation wavelength of 800 nm. Spectra acquisition time was 10 s. At each examined sample site images were obtained using band-pass emission filters at the SHG (400/10 nm) and the TPF (520/40 nm) wavelengths. A wide-pass SBG39 filter (320–654 nm) was also used to collect the combined SHG and TPF signals. The average laser power at the sample was 5 mW. Each acquired image covered an area of $35 \times 35\ \mu m^2$ and was integrated over 10 frames to improve signal to noise ratio.

For each examined sample, the entire thickness of the vessel wall was imaged. To scan the entire thickness of the vessel wall, adjacent images were obtained starting from the intima and moving toward the adventitia in the x-direction for various depths, z. Because of its fragile nature, the endothelium had been lost during excision and it was not imaged. Acquired images were color-coded and tiled together using IPLAB SPECTRUM image-processing software (Scanalytics, Fairfax, VA) to generate a reconstruction of the vessel wall.

Preparation of histological sections

After imaging, each cross-section ring was used for the preparation of a histological section. Histological analysis was performed to facilitate mapping of the different layers in the vessel wall. Thick sections (1 μm) were cut with glass knives perpendicular to the longitudinal axis of the vessel and stained with hematoxylin and eosin for the aorta and toluidine blue O for the coronary arteries. Histological sections were imaged using an Olympus BH-2 upright optical microscope (Nagano, Japan) equipped with an Olympus DP10 camera. In the aorta histological sections, the nuclei of the cells are stained blue-purple, whereas the cytoplasm of the cells, collagen, and elastin have varying degrees of pink staining (Spector et al., 1998.). In the coronary arteries histological sections, the nuclei of cells are stained very dark blue, the cytoplasm is stained blue, collagen is stained light blue/gray, and elastin is stained very light blue/white. The luminal diameter and wall thickness of the coronary vessels were measured using the optical microscope. The acquired images and properties (diameter, wall thickness) of the vessels that were obtained using MPM were compared with the ones obtained from the histological sections for validation.

RESULTS AND DISCUSSION

Characterization of MPM signals from elastic arteries

To first establish the precise origin of image-forming signals from blood vessels, we examined samples of rabbit aorta. Rabbit arteries are highly elastic and their principal components are collagen and elastin in the adventia and media, respectively. Smooth muscle cell content in rabbit elastic arteries is relatively sparse. Images and the corresponding spectra from the same sample site at the same focal plane were acquired from the adventitia (Fig. 1, *a*, *b*, *c,* and *d*), and the media (Fig. 1, *e*, *f*, *g*, and *h*) of the rabbit aortic wall for an excitation wavelength of 800 nm. A broad band filter (320–654 nm) was used to capture both TPF and SHG signals, whereas 400 ± 5 nm and 520 ± 20 nm band-pass filters were used to acquire SHG (*green* color-coded images) and TPF (*red* color-coded images), respectively.

In the adventitia (Fig. 1, *a*, *b*, *c*, and *d*), where collagen is the primary constituent, the images display a strong SHG signal from collagen (Fig. 1 *b*) and a weak TPF signal from elastin (Fig. 1 *c*). The latter cannot be distinguished in the image obtained using a broad emission filter (Fig. 1 *a*). The corresponding spectrum (Fig. 1 *i*, *red*) exhibits a 400-nm SHG signal from collagen and a broad TPF feature spanning

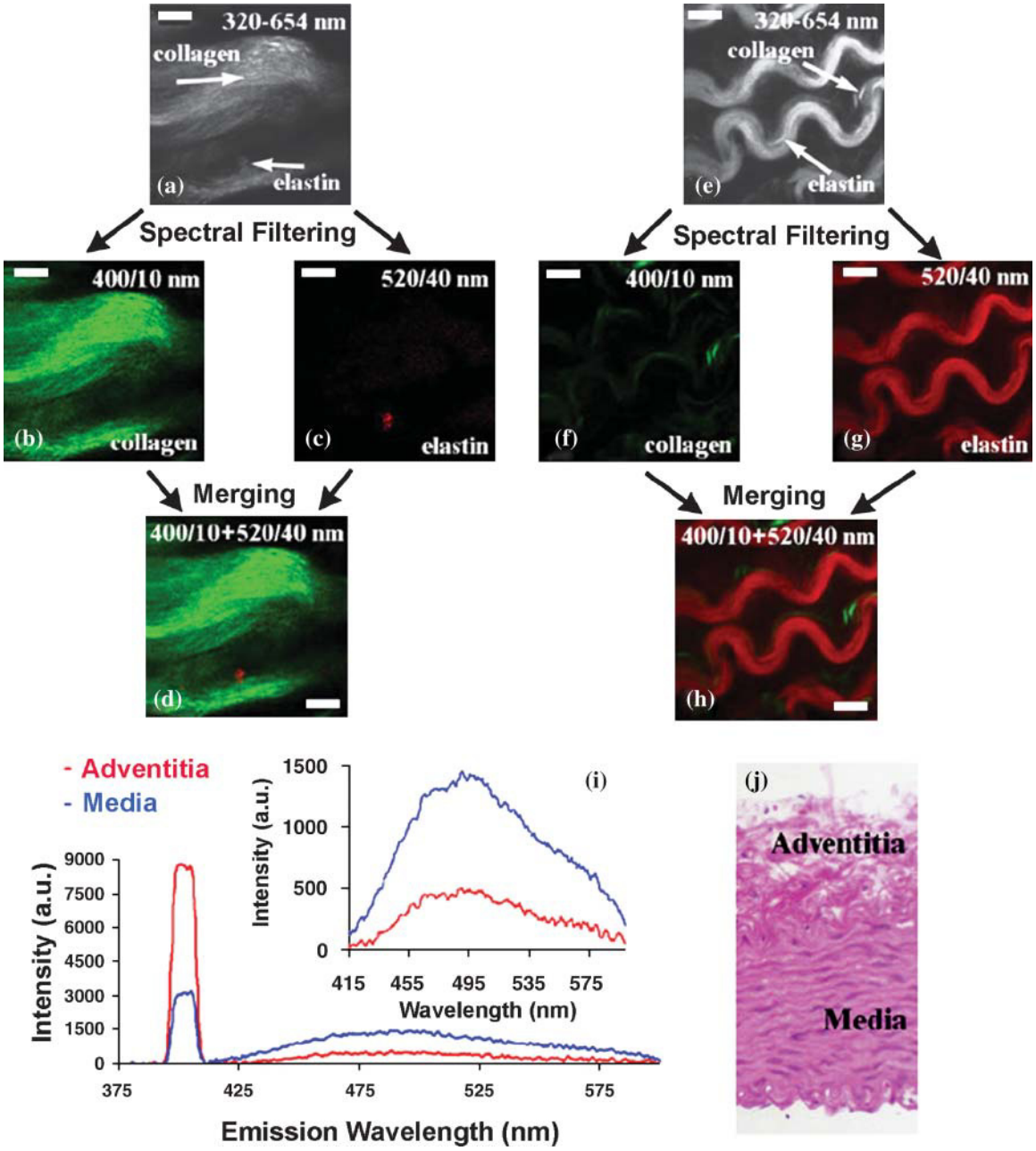

FIGURE 1 Characterization of MPM signals from elastic arteries. MPM images obtained from the same site in the adventitia of the rabbit aortic wall using various emission filters: an SBG39 emission filter (320–654 nm) (*a*), a 400/10-nm filter (*b*), and a 520/40-nm band-pass emission filter (*c*). Overlay image of *b* and *c* is shown in *d*. MPM images obtained from the same focal plane in the media of the rabbit aorta using an SBG39 emission filter (*e*), a 400/10-nm filter (*f*), and a 520/40-nm band-pass emission filter (*g*). Overlay image of *f* and *g* is shown in *h*. Scale bar is 5 μm. Emission spectra corresponding to *a–d* and *e–h* are shown in *i* in red and blue, respectively. Inset in *i* shows TPF spectra alone. Hematoxylin and eosin stained section of rabbit aortic wall (*j*).

the region from ~410–600 nm, with a maximum at ~495 nm (*inset* in Fig. 1 *i*) due to elastin autofluorescence (excitation/emission maxima 410/500 nm; Richards-Kortum and Sevick-Muraca, 1996). The MPM images and spectra show that for an excitation wavelength of 800 nm the signal from collagen is exclusively SHG, whereas TPF originates from elastin, a molecule that approximates a random coil configuration (Mathews et al., 2000), and, therefore, does not generate SHG. We have confirmed the collagen and elastin structures illustrated in the images using conventional histology (Fig. 1 *j*).

In the media (Fig. 1, *e*, *f*, *g*, and *h*), we observe an intense TPF signal from elastin (Fig. 1 *g*) and a weaker SHG signal from collagen (Fig. 1 *f*), which cannot be identified in Fig. 1 *e*. The corresponding spectrum (Fig. 1 *i*, *blue*) exhibits a 400-nm SHG signal of lower intensity compared to that obtained

from the adventitia (Fig. 1 *i*, *red*), reflecting the fact that there are fewer collagen fibers in the media. The TPF signal from the media, however, is significantly higher, corresponding to the greater elastic fiber density in the media. The morphology of the MPM images obtained from the media is consistent with the aorta histology shown in Fig. 1 *j*.

Overlaying the green images (Fig. 1, *b* and *f*, for the adventitia and media, respectively) and red images (Fig. 1, *c* and *g*, for the adventitia and media, respectively), results in high-contrast images that show structural details of the adventitia (Fig. 1 *d*) and the media (Fig. 1 *h*).

Although the images shown herein correspond to fixed specimens, we also examined freshly excised aorta. The fresh and fixed specimens were compared and showed negligible differences. The major effect of fixation was that the elastin fibers in the fixed samples appeared to be curved as compared to the more elongated straight elastin fibers observed in the fresh samples. Similar observations on the effect of fixation of the aorta have been made by Parassasi et al. (2000). The reason elastin fibers acquire a curved shape in the fixed samples is that elastin cannot be fixed (Fung and Sobin, 1981). Hence, although we fix the vessel under distension, once the load is removed, the elastin will recoil and consequently have a tortuous geometry.

Characterization of MPM signals from muscular arteries

To correlate the images of microstructure with the stress state of the vessel wall, we examined the vessel in different mechanical states. Specifically, we examined epicardial coronary arterial segments under four different stress and strain conditions: 1), zero-stress state; 2), no-load (zero-transmural pressure) state; 3), 30-mmHg distension; and 4), 180-mmHg distension. In the zero-stress state, the stress is zero throughout the tissue since all external loads were removed. In the no-load state, the inner wall is under compression whereas the outer wall is in tension because of the existence of residual stress and strain (Fung, 1990). The third and fourth conditions distend the vessel wall to different extents. In each state, we imaged the entire wall thickness of each vessel and performed histological analyses for each specimen to validate the structures imaged by MPM.

Fig. 2 shows a series of images obtained from porcine coronary artery under 30-mmHg distension. The images span the entire thickness of the vascular wall from the intima to the adventitia (Fig. 2, *a–f*). We obtained the MPM images using either a 520/40-nm band-pass emission filter to capture TPF (*red* color-coded images in Fig. 2, *a–f*), and a 400/10-nm band-pass emission filter to isolate SHG (*green* color-coded images in Fig. 2, *a–f*).

After imaging, we performed histological analysis of the vessel (Fig. 2, *g* and *h*) to facilitate mapping of the different layers and structures in the vascular wall. All layers can be seen in the histological section of Fig. 2 *g*. The area imaged by MPM is box-marked on the histological image. We can see a prominent curved internal elastic lamina. The media consists of elongated smooth muscle cells with some collagen fibers between the cells. The collagen fibers are also somewhat elongated as a result of the applied distension in contrast to the zero-stress state where the fiber bundles are more uniform in dimension transmurally (see Fig. 5 *a*). The collagen fibers closer to the lumen are thinner because of larger deformation and stress than the ones closer to the adventitia under this loading condition. The adventitia is rich in collagen bundles, and contains some cells that may be fibroblasts or macrophages. Fig. 2 *h* shows a histology section of the vessel under higher magnification. The areas corresponding to the MPM images of Fig. 2, *a–f,* are box- and letter-marked.

MPM images obtained close to the lumen show a strong TPF signal from a very prominent internal elastic lamina and a weaker TPF signal from smooth muscle cells (Fig. 2, *a* and *b*, *left*). TPF from the smooth muscle cells can most likely be attributed to NAD(P)H and flavin compounds (Schilders and Gu, 1999). The smooth muscle cells are invested with curved collagen fibers that exhibit SHG signal (Fig. 2, *a* and *b*, *right*). In the media, images show TPF from smooth muscle cells (Fig. 2 *c*, *left*) and SHG from thin collagen fibers between the smooth muscle cells (Fig. 2 *c*, *right*). The collagen fibers become thicker in the medial region closer to the adventitia (Fig. 2, *d* and *e*, *right*), suggesting that there exists a nonuniform stress distribution along the vessel wall under this loading condition. In the adventitia (Fig. 2 *f*), SHG is emitted from collagen bundles (Fig. 2 *f*, *right*). A strong TPF signal is detected from small circular structures and thin elastic fibers (Fig. 2*f*, left). The circular structures correspond to elastic fibers oriented in the direction along the vessel axis and are stained white in the histological section of Fig. 2 *h*.

Conventional histology validates the structures illustrated in the MPM images. Specifically, we have shown that the SHG signals detected from coronary arteries are due to collagen, whereas TPF originates from smooth muscle cells and elastin. The TPF signal from elastin appears to be more intense than that of smooth muscle cells. This suggests that elastin may be more efficiently excited at 800 nm.

To establish criteria for the determination of the origin of TPF from the coronary artery wall (i.e., smooth muscle cells, elastin, or both) we investigated the differences between spectra obtained from areas in the vessel wall with various amounts of elastin and smooth muscle cells. Fig. 3 (*top graph*) shows the spectra corresponding to the images of Fig. 2, *a–f*. All spectra exhibit a sharp 400-nm SHG peak with intensity proportional to the collagen content in the images. The TPF signal (Fig. 3, *bottom graph*) spans the region from 415 to 600 nm. For elastin-rich regions with some smooth muscle cells (Fig. 2 *a*) the corresponding TPF spectrum has

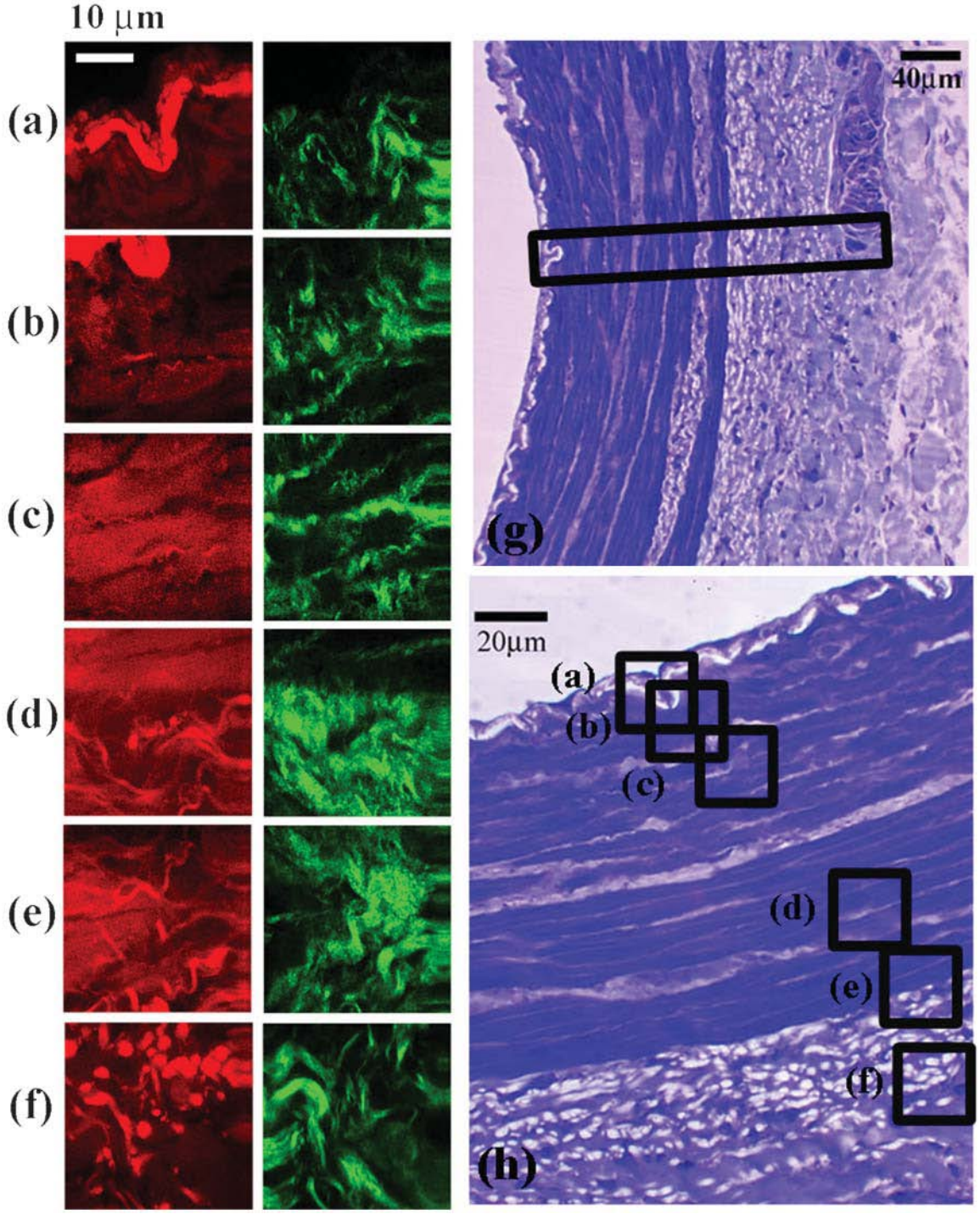

FIGURE 2 Selective visualization of coronary arterial components at pressure of 30 mmHg. MPM images of porcine coronary artery. Images from *a* to *f* span the region from the intima to the adventitia. $\lambda_{ex} = 800$ nm. Red color-coded images correspond to TPF (520/40 nm) and green color-coded images correspond to SHG (400/10 nm). (*g* and *h*) Histology of the imaged vessel. Scanned regions are box-marked.

a maximum at ~510 nm. In spectra obtained from elastin-free regions where TPF is exclusively due to smooth muscle cells (Fig. 2 *c*), the TPF signal has a maximum at 520 nm. This is in good agreement with the TPF maximum of 520 nm that we have previously observed for cellular TPF alone at 800-nm excitation (Zoumi et al., 2002). Spectra acquired from elastin (Fig. 3, *bottom graph*, *green,* and Fig. 1 *g*) have a maximum at 495 nm.

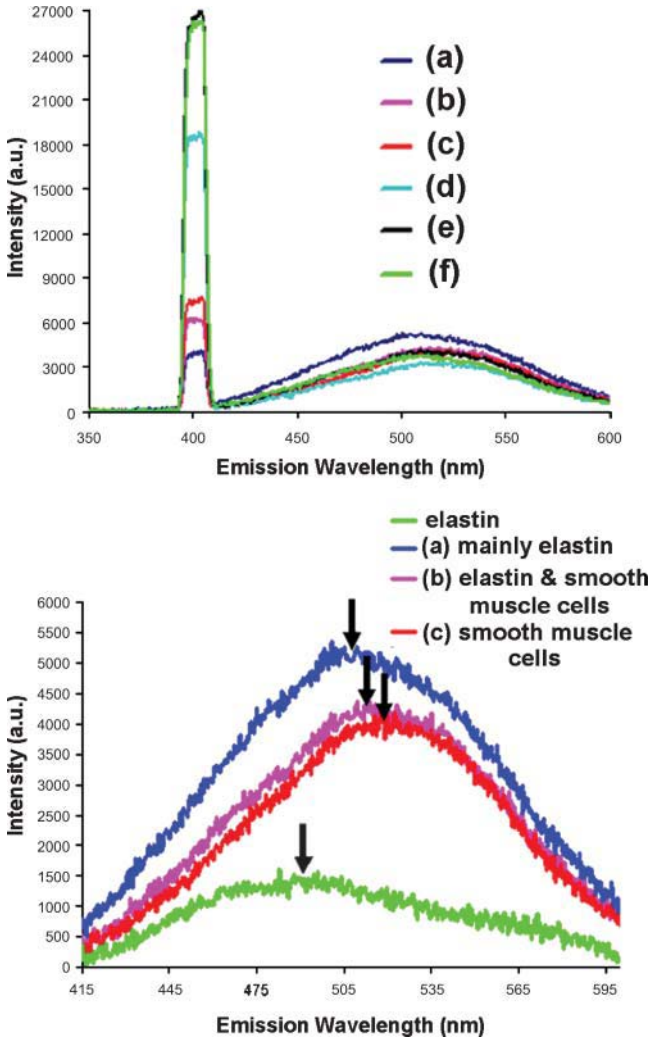

FIGURE 3 Spectral characterization of MPM signals from coronary arteries. Spectra corresponding to images (*a–f*) of Fig. 2 (*top panel*). Bottom panel shows the TPF signal alone. A shift in the TPF maximum (indicated with *arrows*) is observed depending on the elastin and smooth muscle cell content of the scanned region.

Selective arterial imaging over large areas

To use MPM for evaluating the mechanical behavior of coronary arteries we are interested in selectively visualizing the vessel constituents over the entire thickness of the vessel wall. Fig. 4 illustrates an example of the vascular wall reconstruction for a left coronary arterial segment that was subjected to 180-mmHg distension. A low-contrast combined SHG/TPF image (Fig. 4 *a*) is obtained using a broad band-pass emission filter (320–654 nm). The collagen content of the vessel wall can be imaged alone using a 400 nm narrow band-pass filter (Fig. 4 *b*). Similarly, the elastin and smooth muscle cell components of the vessel wall can be isolated from collagen using a 40 nm band-pass emission filter centered at 520 nm (Fig. 4 *c*). Overlaying Fig. 4, *b* and *c*, yields a high-contrast image of the entire coronary artery wall (Fig. 4 *d*). Here, we can clearly distinguish the structure and organization of collagen fibers. The fibers show a regular, parallel organization indicative of the loading that has been applied to the vessel. Fig. 4 *e* illustrates the histology of the vessel. The part of the vessel wall that we scanned shown in Fig. 4, *a–d* is box-marked in Fig. 4 *e*. The structures illustrated in the MPM images are consistent with those from the histological specimens.

Effect of stress state on coronary artery microstructure

Finally, we apply these findings to correlate changes in stress or strain state with alterations in microstructural components. Fig. 5 shows overlay SHG/TPF images of porcine left coronary artery wall from the intima (*left*) to the adventitia (*right*), for various stress states: zero-stress state (Fig. 5 *a*); no-load (zero-transmural pressure) state (Fig. 5 *b*); 30-mmHg distension (Fig. 5 *c*); and 180-mmHg distension (Fig. 5 *d*). We can clearly see the changes in the structure and organization of the vessel constituents under different stress conditions. In Fig. 5, *a* and *b* where no pressure has been applied to the vessel, the fibers are thicker, resulting in a greater overall thickness of the vessel wall. With increasing pressure (Fig. 5, *c* and *d*) the fibers become thinner and more elongated. The overall wall thickness for ten examined specimens exhibited an average % decrease of 65 $\pm$ 22% and 79 $\pm$ 9% when comparing the no-load condition to 30 and 180 mmHg distension, respectively; and an average decrease of 62 $\pm$ 24% and 77 $\pm$ 10% when comparing the zero-stress condition to 30 and 180 mmHg distension, respectively. The error bars have considerable overlap due to the nonuniformity of stress and strain in the no-load and 30 mmHg specimens. The error bars are far smaller for the 180 mmHg case due to the fact that the increased applied pressure (distension) has a more uniform effect throughout the vessel wall. Hence, the vessel wall is radially compressing during pressurization. The elastic lamina, however, is circumferentially stretched. The elastic fibers and smooth muscle cells cannot be clearly resolved in the TPF images. The width of the collagen fibers (SHG images) was measured at three different sites and the average fiber thickness was found to be 3.01 $\pm$ 1.26 μm, 3.63 $\pm$ 1.61 μm, 1.29 $\pm$ 0.47 μm, and 0.93 $\pm$ 0.36 μm for the zero-stress state, the no-load state, the 30-mmHg distension, and the 180-mmHg distension, respectively. The average width of the collagen fibers exhibited a % decrease of $\sim$57% and 69% when comparing the zero-stress condition to 30 and 180 mmHg distension, respectively; and an average decrease of 64% and 74% when comparing the no-load condition to 30 and 180 mmHg distension, respectively. Inspection of Fig. 5 *c* shows that, for the 30-mmHg distension, the portion of the vessel closer to the lumen is affected by the loading more than the region closer to the outer wall. Specifically, the fibers are thinner toward the lumen and become thicker toward the outer wall

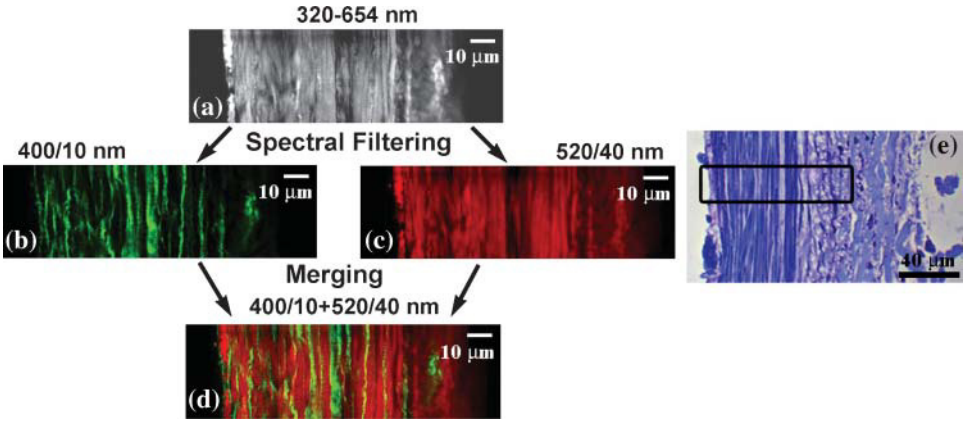

FIGURE 4 Selective imaging of arteries over large areas at pressure of 180 mmHg. Composite images of several adjacent frames of optical sections showing the SHG (*b*), TPF (*c*), and combined SHG/TPF (*a* and *d*) intensities of the matrix fibers in the left anterior descending coronary artery cross-section ring from the intima (*left*) to the adventitia (*right*). MPM images were obtained using various emission filters: an SBG39 emission filter (320–654 nm) (*a*), a 400/10-nm filter (*b*), and a 520/40-nm band-pass emission filter (*c*). Overlay image of *b* and *c* is shown in *d*. Histology section is shown in *e* for comparison. The area marked with the black box corresponds to the imaged area shown in *a–d*.

of the vessel. This effect was also observed in Fig. 2 for a thicker left coronary arterial segment under 30-mmHg distension. In contrast, for the case of 180-mmHg distension (Fig. 5 *d*), the applied pressure seems to have a relatively uniform effect throughout the vessel wall, with thin fibers spanning the entire wall thickness. This observation is consistent with the uniform transmural strain and stress distribution at in vivo loading proposed by Fung and Liu (1992) and Chuong and Fung (1986). They showed that the existence of circumferential residual strain homogenizes the transmural stress distribution at in vivo loading. The stress homogenization is a direct consequence of the fact that the zero-stress state is not equivalent to the no-load state; i.e., there is residual stress and strain in the no-load state when the transmural pressure is zero. Also, relevant to these observations is the fact that the blood vessel wall is a composite structure with different material properties in each layer. Lu et al. (2004) have recently modeled the coronary artery vessel wall as a two layer composite structure consisting of intima-media and adventitial layers. They showed that, at in vivo loading, the intima-media layer is stiffer than the adventitial layer. Furthermore, they found that at lower loading (30 mmHg), the intima-media layer takes up a significant portion of the load as suggested in this study. At higher pressures, the stiffer adventitia is recruited which takes up more of the load.

CONCLUSIONS

The mechanical properties of blood vessels play a critical role in vascular physiology and patho-physiology. In this study we combined simultaneous mechanical loading and visualization of the microstructural components in the same arterial specimen. MPM images and spectra obtained from arteries were shown to provide excellent structural and biochemical characterization of the vessel wall.

A major advantage of using combined SHG/TPF for studying arterial tissue is that it is a noninvasive technique that relies exclusively on endogenous signals, and does not require exogenous probes, which can change the physiologic state of the tissue.

Collagen and elastin affect the mechanical behavior of vessels in different ways. Specifically, collagen contributes mainly to the linear region of the nonlinear stress-strain curve whereas elastin mainly contributes to the toe part of the stress-strain curve. This finding was first reported by Roach and Burton (1957), who used trypsin and formic acid to digest collagen and elastin, respectively, out of blood

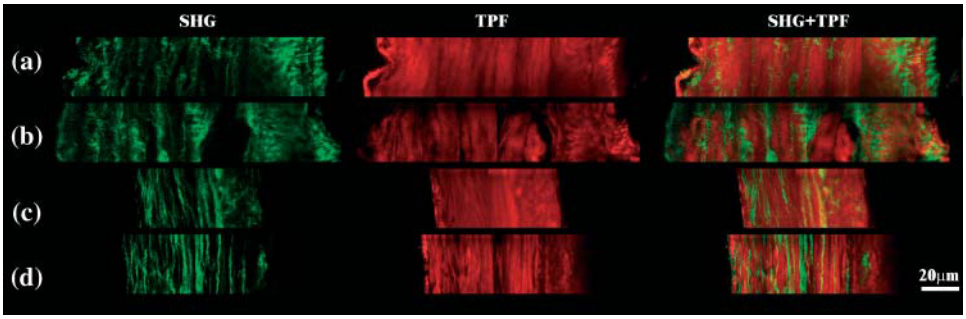

FIGURE 5 Effect of distension on arterial wall micro structure. SHG, TPF, and overlay SHG/TPF composite images of adjacent frames in the same plane of porcine left coronary artery wall from the intima (*left*) to the adventitia (*right*), for various loading conditions: zero-stress state (*a*); no-load (zero-transmural pressure) state (*b*); 30-mmHg distension (*c*); and 180-mmHg distension (*d*).

vessels, but has not been confirmed in intact vessels. Our results show that MPM allows nondestructive selective visualization of various microstructural components in blood vessels and has potential to become a powerful tool in advancing our understanding of vascular biomechanics. In future studies, the stress and strain distributions in the vessel will be computed and correlated with the morphometry of individual fibers. This approach has the potential to enhance our understanding of vascular biomechanics in health and in various disease processes such as hypertension, diabetes, and atherosclerosis.

We thank Dr. Xiaomei Guo for preparation of histological sections.

This work was supported by the National Institutes of Health Laser Microbeam and Medical Program (LAMMP, P41RR-01192), the Air Force Office of Scientific Research, Medical Free-Electron Laser Program (AFOSR MFEL, F49620-00-1-0371), and in part by the National Institutes of Health-National Heart, Lung, and Blood Institute Grant 2 R01 HL055554-06. Dr. Kassab is the recipient of the American Heart Association's Established Investigator Award.

REFERENCES

Agarwal, A., M. L. Coleno, V. P. Wallace, W. Y. Wu, C. H. Sun, B. J. Tromberg, and S. C. George. 2001. Two-photon laser scanning microscopy of epithelial cell-modulated collagen density in engineered human lung tissue. *Tissue Eng.* 7:191–202.

Azuma, T., and M. Hasegawa. 1971. A rheological approach to the architecture of arterial walls. *Jpn. J. Physiol.* 21:37–47.

Azuma, T., and S. Oka. 1971. Mechanical equilibrium of blood vessel walls. *Am. J. Physiol.* 221:1310–1318.

Campagnola, P. J., H. A. Clark, W. A. Mohler, A. Lewis, and L. M. Loew. 2001. Second-harmonic imaging microscopy of living cells. *J. Biomed. Optics.* 6:277–286.

Campagnola, P. J., A. C. Millard, M. Terasaki, P. E. Hoppe, C. J. Malone, and W. A. Mohler. 2002. Three-dimensional high-resolution second-harmonic generation imaging of endogenous structural proteins in biological tissues. *Biophys. J.* 82:493–508.

Campagnola, P. J., M. D. Wei, A. Lewis, and L. M. Loew. 1999. High-resolution nonlinear optical imaging of live cells by second harmonic generation. *Biophys. J.* 77:3341–3349.

Chuong, C. J., and Y. C. Fung. 1986. On residual stresses in arteries. *J. Biomech. Eng.* 108:189–192.

Denk, W., J. H. Strickler, and W. W. Webb. 1990. Two-photon laser scanning fluorescence microscopy. *Science.* 248:73–76.

Diaspro, A., and M. Robello. 2000. Two-photon excitation of fluorescence for three-dimensional optical imaging of biological structures. *J. Photochem. Photobiol. B.* 55:1–8.

Fung, Y. C. 1984. Biodynamics: Circulation. Springer-Verlag, New York.

Fung, Y. C. 1990. Biomechanics: Motion, Flow, Stress, and Growth. Springer-Verlag, New York, Berlin, Heidelberg, London, Paris, Tokyo, and Hong Kong.

Fung, Y. C., and S. Q. Liu. 1992. Strain distribution in small blood-vessels with zero-sress state taken into consideration. *Am. J. Physiol.* 262:H544–H552.

Fung, Y. C., and S. S. Sobin. 1981. The retained elasticity of elastin under fixation agents. *J. Biomech. Eng.* 103:121–122.

Gauderon, R., P. B. Lukins, and C. J. Sheppard. 2001. Optimization of Second-Harmonic Generation Microscopy. *Micron.* 32:691–700.

Gauderon, R., P. B. Lukins, and C. J. R. Sheppard. 1998. Three-dimensional second-harmonic generation imaging with femtosecond laser pulses. *Opt. Lett.* 23:1209–1211.

Georgiou, E., T. Theodossiou, V. Hovhannisyan, K. Politopoulos, G. S. Rapti, and D. Yova. 2000. Second and third optical harmonic generation in type I collagen, by nanosecond laser irradiation, over a broad spectral region. *Opt. Comm.* 176:253–260.

Guo, Y. C., P. P. Ho, H. Savage, D. Harris, P. Sacks, S. Schantz, F. Liu, N. Zhadin, and R. R. Alfano. 1997. Second-harmonic tomography of tissues. *Opt. Lett.* 22:1323–1325.

Guo, Y., H. E. Savage, F. Liu, S. P. Schantz, P. P. Ho, and R. R. Alfano. 1999. Subsurface tumor progression investigated by noninvasive optical second harmonic tomography. *Proc. Natl. Acad. Sci. USA.* 96:10854–10856.

Lu, X., A. Pandit, and G. S. Kassab. 2004. The incremental elastic moduli of coronary artery: a two layer model. *Am. J. Physiol.* In press.

Lu, X., J. B. Zhao, G. R. Wang, H. Gregersen, and G. S. Kassab. 2001. Remodeling of the zero-stress state of femoral arteries in response to flow overload. *Am. J. Physiol. Heart Circ. Physiol.* 280:H1547–H1559.

Masters, B. R., and P. T. C. So. 1999. Multihoton excitation microscopy and confocal microscopy imaging of in vivo human skin: a comparison. *Microsc. Microanal.* 5:282–289.

Masters, B. R., and P. T. C. So. 2001. Confocal microscopy and multiphoton excitation microscopy of human skin in vivo. *Opt. Express.* 8:2–10.

Masters, B. R., P. T. So, and E. Gratton. 1997. Multiphoton excitation fluorescence microscopy and spectroscopy of in vivo human skin. *Biophys. J.* 72:2405–2412.

Masters, B. R., P. T. C. So, and E. Gratton. 1998. Optical biopsy of in vivo human skin: multiphoton excitation microscopy. *Lasers Med. Sci.* 13: 196–203.

Mathews, C. K., K. E. van Holde, and K. G. Ahern. 2000. Biochemistry. Addison Wesley Longman, San Francisco, CA.

Moreaux, L., O. Sandre, M. Blanchard-Desce, and J. Mertz. 2000a. Membrane imaging by simultaneous second-harmonic generation and two-photon microscopy. *Opt. Lett.* 25:320–322.

Moreaux, L., O. Sandre, S. Charpak, M. Blanchard-Desce, and J. Mertz. 2001. Coherent scattering in multi-harmonic light microscopy. *Biophys. J.* 80:1568–1574.

Moreaux, L., O. Sandre, and J. Mertz. 2000b. Membrane imaging by second-harmonic generation microscopy. *J. Opt. Soc. Am. B-Opt. Phys.* 17:1685–1694.

Mulvany, M. J. 1984. Determinants of vascular hemodynamic characteristics. *Hypertension.* 6:13–17.

Oka, S. 1968. Theoretical studies on hemorheology. The 16th Rheology Symposium. Zairyo, Tokyo, Japan.

Oka, S. 1972. Some theoretical studies on hemorheology. *In* Advances in Biophysics. University of Tokyo Press, Tokyo. 97

Oka, S. 1981. Cardiovascular Hemorheology. Cambridge University Press, Cambridge.

Oka, S., and T. Azuma. 1970. Physical theory of tension in thick walled blood vessels in equilibrium. *Biorheology.* 7:109–117.

Parasassi, T., W. Yu, D. Durbin, L. Kuriashkina, E. Gratton, N. Maeda, and F. Ursini. 2000. Two-photon microscopy of aorta fibers shows proteolysis induced by LDL hydroperoxides. *Free Radic. Biol. Med.* 28:1589–1597.

Richards-Kortum, R., and E. Sevick-Muraca. 1996. Quantitative optical spectroscopy for tissue diagnosis. *Annu. Rev. Phys. Chem.* 47:555–606.

Roach, M. R., and A. C. Burton. 1957. The reason for the shape of the distensibility curves of arteries. *Can. J. Biochem. Physiol.* 35:681–690.

Roth, S., and I. Freund. 1981. Optical second-harmonic scattering in rat-tail tendon. *Biopolymers.* 20:1271–1290.

Schilders, S. P., and M. Gu. 1999. Three-dimensional autofluorescence spectroscopy of rat skeletal muscle tissue under two-photon excitation. *Appl. Opt.* 38:720–723.

So, P. T. C., H. Kim, and I. E. Kochevar. 1998. Two-photon deep tissue ex vivo imaging of mouse dermal and subcutaneous structures. *Opt. Express*. 3:339–350.

Spector, D. L., R. D. Goldman, and L. A. Leinwand. 1998. Cells. A Laboratory Manual. Cold Spring Harbor Laboratory Press, Cold Spring Harbor, NY.

Squirrell, J. M., D. L. Wokosin, J. G. White, and B. D. Bavister. 1999. Long-term two-photon fluorescence imaging of mammalian embryos without compromising viability. *Nature Biotech.* 17:763–767.

Zoumi, A., A. Yeh, and B. J. Tromberg. 2002. Imaging cells and extracellular matrix *in vivo* by using second-harmonic generation and two-photon excited fluorescence. *Proc. Natl. Acad. Sci. USA*. 99:11014–11019.